Inorganic Chemistry

Article

pubs.acs.org/IC

Labile Degree of Disorder in Bismuth-Oxophosphate Compounds: Illustration through Three New Structural Types

A. Aliev,[†] D. Endara,[†] M. Huvé,[†] M. Colmont,[†] P. Roussel,[†] L. Delevoye,[†] T.T. Tran,[‡] P.S. Halasyamani,[‡,§] and O. Mentré*[,†]

[†]Université Lille Nord de France, UMR 8181 CNRS, Unité de Catalyse et de Chimie du Solide (UCCS USTL), F-59655 Villeneuve d'Ascq, France

[‡]Department of Chemistry, University of Houston, Houston, Texas 77204-5003, United States

[§]Department of Chemistry, Aalto University, Kemistintie 1 FI-02150 Espoo, Finland

Supporting Information

ABSTRACT: Here, we analyze the crystal structures of three new Bi/M oxophosphates, focusing on the ambiguity between order and disorder in different structural subunits. The three structures are original but systematically built on the assembly of $O(Bi,M)_4$ tetrahedra into various 1D-oxocenterd units, separated by PO_4 groups that create cationic channels. Two main subunits show versatile degrees of disorder, i.e., the cationic channels and some of the terminal $O(Bi,M)_4$ entities. (a) In the compound $[Bi_2(Bi_{1.56}K_{0.44})^{dis}O_3]K_{0.88}{}^{dis}(PO_4)_2$, the K/K and K/Bi disorder is total on both *nano-* and *micro*-sized domains. (b) In the incommensurately modulated $[Bi_{10}(Bi_{\sim 0.5}Cd_{\sim 0.5})_8{}^{dis}O_{16}](Bi_{0.6}Cd_{0.8})_2{}^{ord}(PO_4)_8$, only the cationic channels show an ordered Bi/Cd arrangement which can be modified by minor stoichiometric changes between domains. (c) In $[Bi_{18}Zn_{10}O_{21}]^{ord}Zn_5{}^{ord}(PO_4)_{14}$, both subunits are almost perfectly ordered (complex Bi/Zn sequence) into a 7-fold supercell, but this order strongly depends on the observation scale and is mainly lost in micronic-grains also due to slight compositional changes. However, the refined noncentrosymmetric organization is maintained (SHG tests) in the bulk. The relative stability of ordered versus disordered sites is discussed on the basis of the existence of two possible mixed sites and probably depends on the M chemical nature. Disorder was characterized by use of solid-state ^{31}P NMR probing for the first two cases. Finally, the observed disordered or long periodicities along the infinite dimension suggest the sketch of a periodic/rigid skeleton of $O(Bi,M)_4$ units with counterions filling the interspace in more or less disordered arrangements.

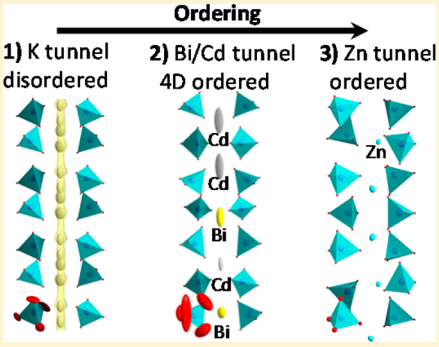

INTRODUCTION

Bismuth oxides and oxy-salts demonstrate a great structural diversity due to the often-found OBi_4 units able to organize into zero-dimensional (0D), 1D, 2D, and 3D frameworks.[1] However, the typical Bi^{3+}−O bond valence is 0.596 valence units (v.u.), which is slightly higher than the 0.5 v.u. needed to form an ideal OBi_4 tetrahedron.[2] As a result, the OBi_4 tetrahedra are usually strongly distorted, or admit the copresence of a different cation M^{n+} into $O(Bi,M)_4$ tetrahedra, whose M−O contribution is relaxing the central oxygen bond valence sum. The great diversity of aliovalent M cations that can be incorporated into the $O(Bi,M)_4$ tetrahedral bricks make this class of inorganic compounds a gold mine of inspiration for the findings of novel structural motifs and physical properties. The literature abound in compounds with oxocentered Bi/M/O based units assembled into various topologies, such as 1D-columns,[3,4] crenel-planes,[5] 3D-porous frameworks,[6] etc. (see ref 1 for a review). Particularly, the Bi_2O_3−MO−P_2O_5 (M = divalent metals) ternary system displays an impressive number of distinct crystal structures based on the association of $O(Bi)_4$ and $O(Bi,M)_4$ into versatile subunits.[7−10] In most cases, they are linked by sharing edges into infinite *n*-tetrahedra-wide 1D-polycationic ribbons. These units are separated by phosphate groups, with respect to systematic unified "rules" that allow the prediction/formulation and realization of novel original terms.[11] For instance, we have recently "*designed*" novel noncentrosymmetric (NCS) compounds by predicting the NCS arrangement between polar ribbons (n = 5, 3, and 11 tetrahedra wide),[8] as well as the infinite layered term ($n\rightarrow\infty$) of formula $[Bi_2O_2][BiO]_2M(PO_4)_2$ (M = Mg, Zn).[9]

Two main reasons are responsible for the possibility to tune the size and the shape of the ribbons in a tailor-made manner: (a) The strong analogy of these compounds with the fluorite-like δ-Bi_2O_3 crystal structure that corresponds to a 3D-pavement of edge-sharing oxocentered OBi_4 and vacant $\square Bi_4$ tetrahedra.[12] After substitution in this parent structure of Bi for M cations and PO_4 groups, labile clusters of $O(Bi,M)_4$ oxocentered units are preserved isolated by PO_4.[8,10,13] (b) The stability in this cationic sublattice of mixed sites and the

Received: August 27, 2013
Published: December 27, 2013

Table 1. Crystal Data, Measurement, and Structural Refinement Parameters for $[Bi_2(Bi_{1.56}K_{0.44})^{dis}O_3]$ $K_{0.88}{}^{dis}(PO_4)_2$, $[Bi_{18}Zn_{10}O_{21}]^{ord}Zn_5{}^{ord}(PO_4)_{14}$, and $[Bi_{10}(Bi_{\sim 0.5}Cd_{\sim 0.5})_8{}^{dis}O_{16}](Bi_{0.6}Cd_{0.8})_2{}^{ord}(PO_4)_8$

	$[Bi_2(Bi_{1.56}K_{0.44})^{dis}O_3]$ $K_{0.88}{}^{dis}(PO_4)_2$	$[Bi_{18}Zn_{10}O_{21}]^{ord}$ $Zn_5{}^{ord}(PO_4)_{14}$	$[Bi_{10}(Bi_{\sim 0.5}Cd_{\sim 0.5})_8{}^{dis}O_{16}]$ $(Bi_{0.6}Cd_{0.8})_2{}^{ord}(PO_4)_8$
	crystal data		
crystal symmetry	tetragonal	orthorhombic	tetragonal
space group	$P\bar{4}2_1c$	I2mb	$I4/m(00\gamma)$s0
a (Å)	13.7008(2)	14.8003(1)	13.7595(6)
b (Å)	13.7008(2)	38.0848(2)	13.7596(6)
c (Å)	5.6633(1)	1.2473(5)	5.6879(3)
V (Å^3)	1063.07(2)	6339.7(3)	1076.85(9)
			q-vector 0 0 0.3984(2)
Z	4	4	1
Dx (g/cm3)	6.421	6.711	7.423
μ(mm^{-1})(0.7107 Å)	58.72	55.81	65.14
appearance	colorless needle	colorless needle	colorless needle
crystal size (mm)	0.33 × 0.07 × 0.05	0.47 × 0.05 × 0.04	0.09 × 0.04 × 0.04
	data collection		
λ(Mo Kα)(Å)	0.71073	0.71073	0.71073
scan mode	ω and φ	ω and φ	ω and φ
θ(min−max) (deg)	2.1−37.6	1.9−28.3	1.64−27.5
R(int) (%)	5.4	5.6	9.5
reciprocal space	$-22 \le h \le 23$	$-19 \le h \le 19$	$-17 \le h \le 17$
recording	$-21 \le k \le 22$	$-50 \le k \le 50$	$-17 \le k \le 17$
	$-7 \le l \le 9$	$-14 \le l \le 14$	$-8 \le l \le 8$
			$-2 \le m \le 2$
	refinement		
meas., obs./indep. all (obs = $I > 3\sigma(I)$)	32075, 2261/2677	63040, 6895/7947	30811, 898/3152
			main obs/all 510/686
			1st sat. obs/all 361/1227
			2nd sat. obs/all 27/1239
no. of refined parameters	88	391	162
refinement method	F	F	F
R1(F^2)(obs)/ R1(F^2)(all) (%)	3.14/4.19	3.70/4.45	main obs 3.89
			1st sat. obs 10.97
			2nd sat. obs 13.37
wR2(F^2)(obs) /wR2(F^2)(all) (%)	3.64/6.18	4.01/4.53	main obs 5.48
			1st sat. obs 11.13
			2nd sat. obs 14.67
GOF(obs)/GOF(all)	2.20/3.42	1.37/1.43	2.88/1.65
$\Delta\rho_{max}$/ $\Delta\rho_{min}$ (e Å^{-3})	3.29 /−2.80	3.08 /−2.80	6.97/−4.49
extinction coefficient	0.1800 (40)	0.0155 (5)	0.00049(3)

creation of interstitial channels with aliovalent Bi^{3+}/M^{n+} cations. Such sites can be tuned in terms of their relative Bi/M occupancies for charge balance.

This leads to extended series of very particular compounds, at least crystallographically, where the oxocentered clusters form a well-organized periodic lattice despite the presence of mixed Bi/M sites, while the surrounding medium (PO_4 and interstitial channels) can be strongly disordered.[14] For instance, we have recently described two novel disordered crystal structures in the Bi_2O_3−CuO−P_2O_5 system with intergrowths between n = 4 and n = 3 wide ribbons.[10] In the absence of systematic arguments for the existence or not of long-range or medium-range ordering, we have defined some of the compounds as crystalline-glassy intermediates on the basis of ^{31}P NMR experiments.[15] These results comfort a general sketch that the crystallinity of these compounds is held by a rigid O(Bi,M)$_4$ skeleton, while interstices are filled by disordered counterions (XO_4 groups or interstitial cations). However, we have sometimes observed the evidence of modulated structures either by electron diffraction[7,16] or on XRD single crystal patterns[17] that denote a partial or complete ordering into large periodicities. Such ordering could occur in small-sized domains but also extend to a larger scale, e.g., "standard" micrometric size of single crystals. Taking into account the number of concerned compounds, this ambiguity between full ordering and partial or complete disorder deserves attention. Here, we present three new structural types that cover the full panorama: $[Bi_2(Bi_{1.56}K_{0.44})^{dis}O_3]K_{0.88}{}^{dis}(PO_4)_2$, $[Bi_{10}(Bi_{\sim 0.5}Cd_{\sim 0.5})_8{}^{dis}O16](Bi_{0.6}Cd_{0.8})_2{}^{ord}(PO_4)_8$, and $[Bi_{18}Zn_{10}O_{21}]^{ord}Zn_5{}^{ord}(PO_4)_{14}$, where *dis* and *ord* stand for disordered and ordered subunits, respectively.

EXPERIMENTAL SECTION

$[Bi_2(Bi_{1.56}K_{0.44})^{dis}O_3]K_{0.88}{}^{dis}(PO_4)_2$. Single crystals of $[Bi_2(Bi_{1.56}K_{0.44})^{dis}O_3]K_{0.88}{}^{dis}(PO_4)_2$ were found in a polyphasic residue obtained as follows: The mixture 0.5K_2CO_3 + 2.5 Bi_2O_3 + 2$(NH_4)_2HPO_4$ was ground and loaded into a gold tube with one end left open, which was heated up to 900 °C (rate 50 °C/h), then left for a 10 h plateau, cooled down slowly to 600 °C (rate 3 °C/h), and finally the furnace was switched off. Electron microprobe analysis has

dx.doi.org/10.1021/ic402930d | Inorg. Chem. 2014, 53, 861−871

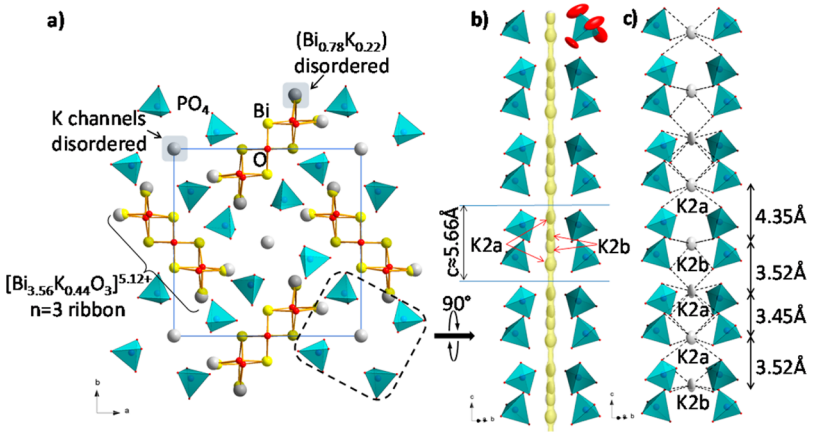

Figure 1. (a) Projection along the *c* axis of the crystal structure of $[Bi_2(Bi_{1.56}K_{0.44})^{dis}O_3]K_{0.88}{}^{dis}(PO_4)_2$. (b) Representation of the channels (the yellow continuum along the tunnel is the electron density obtained after Fourier difference of the electron map without K (14 $e^-/Å^3$) and (c) hypothetic possible K arrangement along the *c* axis.

given the following: 1.3:3.4:2 for K/Bi/P, which is very close to refined occupations.

Polycrystalline samples have been prepared for several stoichiometries around the one from single crystal XRD $[Bi_2(Bi_{1.56}K_{0.44})^{dis}O_3]$-$K_{0.88}{}^{dis}(PO_4)_2$, to validate the refined chemical composition. The procedure is as follows: the stoichiometric amounts of K_2CO_3, Bi_2O_3, and $(NH_4)_2HPO_4$ were ground together and loaded into an alumina crucible, then heated at 400 °C for 10 h and at 860 °C for 48 h with intermediate grindings. Our results suggest that the cooling rate is not a decisive parameter.

$[Bi_{10}(Bi_{\sim 0.5}Cd_{\sim 0.5})_8{}^{dis}O_{16}](Bi_{0.6}Cd_{0.8})_2{}^{ord}(PO_4)_8$. Single crystals were isolated in a melted sample of initial composition $Bi_4CdP_2O_{12}$. The mixture CdO + $2Bi_2O_3$ + $2(NH_4)_2HPO_4$ was ground and loaded into a gold tube with one end left open, which was heated up to 950 °C (rate 50 °C/h), then left for a 10 h plateau and cooled down slowly to 600 °C (rate 3 °C/h), and finally the furnace was switched off. The EDX analysis has given values close to the refined formula, namely: 15.6:5.3:8 for Bi/Cd/P, respectively.

Powder was prepared according to the following protocol: stoichiometric amounts of CdO, Bi_2O_3, and $(NH_4)_2HPO_4$ were ground together and placed into an alumina crucible. The crucible was heated at 400 °C for 10 h then at 880 °C for 48 h with intermediate grindings. Finally, the sample was cooled down to 400 °C over 3 h, after which the furnace was switched off.

$[Bi_{18}Zn_{10}O_{21}]^{ord}Zn_5{}^{ord}(PO_4)_{14}$. Colorless needles of $[Bi_{18}Zn_{10}O_{21}]^{ord}Zn_5{}^{ord}(PO_4)_{14}$ were picked out from a polyphasic residue obtained according to the following protocol: the mixture ZnO + $0.5Bi_2O_3$ + $(NH_4)_2HPO_4$ was ground together and loaded into a gold tube with one end left open, heated up to 900 °C at a rate of 50 °C/h, then left over 10 h and cooled down to 600 °C at a rate 3 °C/h, after which the furnace was switched off. The EDX analysis has given the following approximate elemental ratio 18.2:14.9:14 for Bi/Zn/P.

A powder sample was prepared by heating the mixture, obtained by grinding together the stoichiometric amounts of ZnO, Bi_2O_3, and $(NH_4)_2HPO_4$, at 400 °C for 10 h then at 800 °C for 48 h with intermediate grindings. Several syntheses also suggested that the cooling rate is not important.

Single crystal XRD data of all the investigated samples have been collected using a Bruker Apex Duo diffractometer with a Mo–IμS microfocus tube (λ = 0.71073 Å). The intensity data have been extracted from the collected frames using the program SAINT-Plus 8.27b.[18] The lattice parameters have been defined from the complete data set. Absorption corrections have been performed using multiscan methods with SADABS.[19] The structures were solved with the Superflip crystal structure solving computer program.[20] The Jana2006 program was used for structure refinements.[21] The data collection and pertinent data of the refinements for all single crystals studied in this work are gathered in Table 1; also see Tables S1–S7 (Supporting Information) for atomic displacement parameters.

Powder X-Ray Diffraction. Powder X-ray diffraction analyses of all the powder samples were performed at room temperature in a 2θ range of 5–60° with a scan step width of 0.02° using a D8 Advance Bruker AXS diffractometer (Cu Kα radiation, λ = 1.5418 Å). XRD pattern profile fitting was fitted with the Fullprof program[22] for standard structures and with JANA2006[21] for modulated ones.

Solid-State NMR. Solid-state NMR analyses were performed under magic angle spinning (MAS) at 20 kHz (3.2 mm probehead) on an 18.8 T Bruker spectrometer operating at 323.87 MHz for the ^{31}P nucleus.

Transmission Electron Microscopy. Electron Diffraction Patterns (EDP) have been obtained on an FEI Technai G220 transmission electron microscope equipped with a precession system. The material was crushed and dispersed on a holey carbon film deposited on a Cu grid.

Second–Harmonic Generation. Powder SHG measurements were performed on a modified Kurtz–NLO system using a pulsed Nd:YAG laser with a wavelength of 1064 nm. A detailed description of the equipment and methodology has been published elsewhere.[23] As the powder SHG efficiency has been shown to depend strongly on particle size, the reported materials were ground and sieved into distinct particle size ranges (<20, 20–45, 45–63, 63–75, 75–90, >90 μm). Comparisons with known SHG materials were made by grinding and sieving crystalline α-SiO_2 and $LiNbO_3$ into the same particle size ranges. No index matching fluid was used in any of the experiments.

RESULTS AND DISCUSSION

1. Complete Disorder in $[Bi_2(Bi_{1.56}K_{0.44})^{dis}O_3]$-$K_{0.88}{}^{dis}(PO_4)_2$. The compound $[Bi_2(Bi_{1.56}K_{0.44})^{dis}O_3]$-$K_{0.88}{}^{dis}(PO_4)_2$ is a pertinent example of a "fully disordered" prototype, in the sense that several subunits assembled in the crystal structure all show statistic distribution over mixed sites (edges) or over adjacent positions (PO_4 groups and tunnels) while diffraction patterns show no evidence of any ordering (extra spots) nor pseudo-ordering (diffuse streaks). The crystal structure was solved in the $P\bar{4}2_1c$ space group (a = 13.7008(2) Å, c = 5.6633(1) Å) with final reliability factors R_1 = 3.14% and wR_2 = 3.64%. The crystal structure is built of triple, n = 3, oxocentered tetrahedra long ribbons, each surrounded by eight PO_4 groups while projected in the (a, b) plane (see Figure 1a).

The formula of the 1D ribbons is $[Bi_{3.56}K_{0.44}O_3]^{5.12+}$ in which the site at the edges of the ribbon is mixed and is refined to $[Bi_{0.78}K_{0.22}]$. For this refinement, due to a close Fourier-difference peak, the full occupancy was restrained while K and

dx.doi.org/10.1021/ic402930d | Inorg. Chem. 2014, 53, 861–871

Bi atomic coordinates were free-refined but restrained to equal thermal parameters. The initial refined occupancy close to Bi/K = 0.85:0.15 was finally fixed in the last cycles to 0.78:0.22 without significant increasing of R values, in order to reach electroneutrality taking into consideration the occupancy of the interstitial K^+ channels by PO_4 walls. Fourier difference maps (in the absence of cations in the tunnel) show a continuum of electron density shown in yellow in Figure 1b, for an isoelectronic level of 14 $e^-/Å^3$. Two broader positions are highlighted along the c axis, which correspond to two crystallographic sites K2a (44% occupied) and K2b (44% occupied). Restrained to equal ADPs. The total occupancy of the channels (~88%) leads to an average number of cations = 1.76 per tunnel, i.e., along the c axis (5.66 Å) with a mean K−K distance of 3.21 Å (= 5.66/1.76) which is a reasonable K−K separation length. The deduced $[Bi_2(Bi_{1.56}K_{0.44})^{dis}O_3]K_{0.88}{}^{dis}(PO_4)_2$ was confirmed by further syntheses of the polycrystalline sample detailed below. The pertinent distances are listed in the Table 2.

Table 2. Selected Interatomic Distances (Å) in $[Bi_2(Bi_{1.56}K_{0.44})^{dis}O_3]K_{0.88}{}^{dis}(PO_4)_2$

atom 1	atom 2	d	atom 1	atom 2	d
Bi1	1xO5	2.246(16)	K2a	2xO1	2.760(41)
	1xO5	2.278(16)	K2b	2xO4	2.592(40)
	1xO3	2.374(20)		2xO4	2.610(30)
	1xO3	2.476(28)	P1	1xO4	1.482(29)
	1xO1	2.485(28)		1xO1	1.493(27)
	1xO4	2.760(28)		1xO3	1.506(20)
K1	1xO1	2.401(35)		1xO2	1.531(19)
	1xO5	2.415(26)			
	1xO4	2.469(34)			
	1xO3	2.540(36)			
	1xO3	2.546(30)			
	1xO5	2.589(25)			
Bi2	1xO6	2.154(9)			
	1xO5	2.269(16)			
	1xO2	2.401(22)			
	1xO5	2.495(16)			
	1xO2	2.528(20)			
	1xO6	2.545(12)			

In Figure 1c, a hypothetical K2a/K2b sequence along c is shown with respect to the occupancies of K2a and K2b. Of course, a diversity of different pseudo-ordered arrangements of this kind is possible and should coexist locally, but without any correlation since no superstructure spots are observed. It is noteworthy that the coordination of the K^+ ions by PO_4 corners leads to reasonable K−O distances. Bond valence sum (BVS) calculations lead to 0.75 and 0.96 for K2a and K2b, both slightly underbonded. Clearly, the oxygen atoms involved in K−O bonds (O1, O2, O3, and O4) have large thermal parameters (see Figure 1b), which probably pictures the existence of satellite PO_4 positions tilted around the refined one. It is probable that the exact PO_4 orientation depends on the local neighbors' atomic surrounding both at edges of ribbons (K1 versus Bi1) and in the tunnels (K2a versus K2b).

Concerning the ribbon edges, using the refined PO_4 position, the calculated BVS for Bi1 and K1 gave respectively 2.62 and 1.73. Clearly, the value obtained for Bi1 matches rather well to the expected +3 value, while the K1 coordination is not suitable. The mixed Bi1(78%)/K1(22%) being dominated by the occupancy of the former, the positions of coordinating PO_4 corners for local K1 presence is not accurately probed. Once more, this can be related to the high values of the thermal parameters for the bordering PO_4. Finally, the high thermal parameters of the PO_4 corners reinforce the full disordered nature of $[Bi_2(Bi_{1.56}K_{0.44})^{dis}O_3]K_{0.88}{}^{dis}(PO_4)_2$. Indeed, the precession frame (see Figure 2a), calculated using single crystal

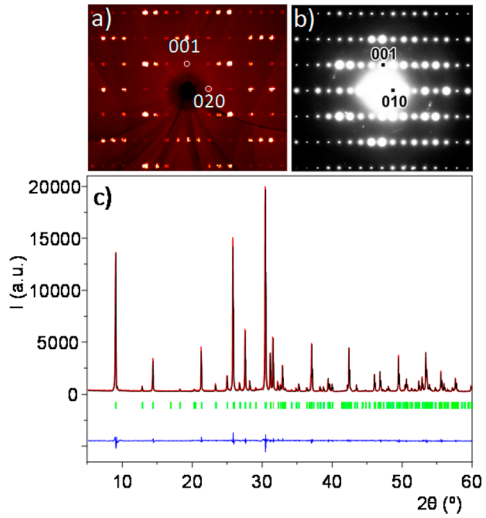

Figure 2. $[Bi_2(Bi_{1.56}K_{0.44})^{dis}O_3]K_{0.88}{}^{dis}(PO_4)_2$: (a) calculated precession frame of the 0kl layer from single crystal XRD data. (b) ED patterns of the corresponding compound. (c) Profile fitting of the corresponding powder (refined unit cell parameters a = 13.6922(3) Å, c = 5.6602(2) Å, V = 1061.16(4) $Å^3$, χ^2 = 2.25).

XRD data, shows a good crystallinity in the absence of any extra spots or diffuse streaks. In addition, the ED patterns of the corresponding powder (Figure 2b) do not show any clue of ordering even at this observation scale, which is much lower than for a single crystal (a few nanometers compared to a few micrometers). Note also that the diffractogram of $[Bi_2(Bi_{1.56}K_{0.44})^{dis}O_3]K_{0.88}{}^{dis}(PO_4)_2$ shows the unique expected phase (see Figure 2c).

The disorder around P centers can be characterized by use of solid-state ^{31}P NMR probing the local environment of nuclei. In a general way, under optimum MAS and pulse decoupling conditions, ordered crystal structures are characterized by resonances line widths that do not exceed a few hundred hertz, best fitted with a Lorentzian profile. In disordered compounds, the distribution of geometric parameters around a single site induces chemical shift changes that result in a Gaussian resonance broadening. Figure 3a shows the ^{31}P MAS NMR spectra of $[Bi_2(Bi_{1.56}K_{0.44})^{dis}O_3]K_{0.88}{}^{dis}(PO_4)_2$. The ^{31}P MAS NMR can be separated into two main groups of resonances, dominated by a Gaussian distribution, centered at −2.1 and 0.4 ppm with a ratio of 55:45, together with one of lower intensity around 3 ppm. This latter is assigned to minor PO_4 containing impurities, and its line width of about 900 Hz can be used as a reference in favor of a disordered character of the pertinent phase, especially keeping in mind the unique P crystallographic site. The chemical shift result from cationic effects as already reported for the disordered $Bi_{\sim 1.2}Zn_{\sim 1.2}O_{1.5}(PO_4)$[15] and $BiMg_{2-x}Cd_xPO_6$ solid solutions.[24] Taking into account the first K/Bi disordered cationic sphere (P−K/Bi < 5 Å), four K2/Bi2 sites participate. A statistic K/Bi distribution involves P−Bi_4 (31.2%), P−Bi_3K_1 (25.6%), P−Bi_2K_2 (20%), P−Bi_1K_3 (14.4%),

dx.doi.org/10.1021/ic402930d | Inorg. Chem. 2014, 53, 861−871

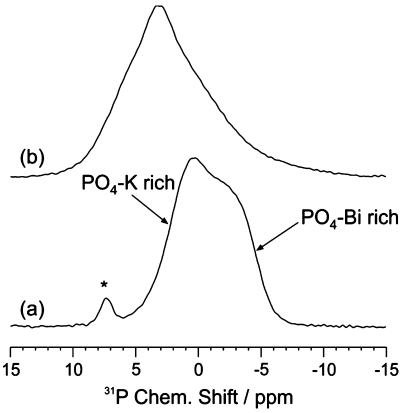

Figure 3. ^{31}P MAS spectra at 18.8 T of (a) $[Bi_2(Bi_{1.56}K_{0.44})^{dis}O_3]K_{0.88}{}^{dis}(PO_4)_2$ and (b) $[Bi_{18}Zn_{10}O_{21}]^{ord}Zn_5{}^{ord}(PO_4)_{14}$. In a, the star (*) denotes an impurity phase. The spectra were acquired with a total of 32 scans, a short pulse excitation of 0.8 μs and a recycling delay of 10 s.

and P−K_4 (8.8%). In our approach, the K2a/K2b disorder inside the tunnels is considered as an extra degree of resonance broadening. The ^{31}P NMR chemical shift expected between K and Bi second neighbors can be related to the electronegative effect on P−O bonds through the z/a^2 parameter, where z is the cationic charge and a the mean X−O interatomic (rO + rX).[24,25] We calculate z/a^2 = 0.52 and 0.12 for Bi and K, respectively. Therefore, the two main resonances at −2.1 and 0.4 ppm are accounted for by Bi-rich and K-rich coordinations, respectively,[24] in good agreement with experimental weights and statistic values. The ^{31}P double-quantum MAS NMR spectrum (see Figure S1 in the SI), with important diagonal and out-of diagonal intensities, highlighting those phosphate groups that are close to each other in the absence of segregation, provides further indication on the real disordered structure of $[Bi_2(Bi_{1.56}K_{0.44})^{dis}O_3]K_{0.88}{}^{dis}(PO_4)_2$.

Our results validate a full random statistic distribution over all disordered crystallographic positions, while the rigid/periodic framework is achieved by the oxocentered ribbon units. It makes sense to consider channel hosts and PO_4 groups as counterions that make the cohesion between the periodic $O(Bi,K)_4$ based skeleton. Comparing the structure of $[Bi_2(Bi_{1.56}K_{0.44})^{dis}O_3]K_{0.88}{}^{dis}(PO_4)_2$ with that of $Bi_2PbMnO_4(PO_4)_2$,[17] one can note a similar topology between n = 3 ribbons. The formula of this compound was later revised into $[Bi_2(Pb,Mn)_2{}^{dis}O_3](Pb,Mn)_{0.6}{}^{ord}(PO_4)_2$ with both the edges of ribbons and the channels hosting mixed Pb^{2+}/Mn^{2+} cations. The refinement of the structure in $P\bar{4}2_1c$ (a = 13.275(3) Å, c = 5.500(2) Å) also shows several tetrahedral configurations disordered around the central phosphorus site. In fact, this compound displays a modulated structure and was refined, in a further stage, in the super space group Xcc2(00γ)s0s (R_{fund} = 4.56% and $R_{satellite}$ = 12.7%).[26] It shows disordering of Pb and Mn at edges of ribbons while Pb and Mn were found fully ordered in the cationic channels. It follows that the cationic nature could also be a key factor for ordering or not in those structures. Particularly, the ionicity of M−O bonds could be involved, since ionic K^+−O do not involve axial cationic orbitals leading to versatile coordinations in the same crystal (e.g., K2a vs K2b) in the absence of ordering, comparatively to more rigid Mn^{2+} coordination. For this particular compound, the disorder would be intrinsic, since several batches lead to similar results. Also the absence of any diffuse streaks in ED patterns of crushed crystals and powders indicates no K−K correlation in the channels.

2. Partial Cationic Ordering in the 1D Square-Columns Compound $[Bi_{10}(Bi_{\sim0.5}Cd_{\sim0.5})_8{}^{dis}O_{16}]$-$(Bi_{0.6}Cd_{0.8})_2{}^{ord}(PO_4)_8$. In this compound, contrarily to the previous case, we show evidence of an intermediate situation with fully ordered tunnels which generate a structural modulation and disordered mixed Bi/Cd edges at the edges of columnar oxocentered clusters. A colorless needle was selected for single crystal XRD data collection. The average crystal structure (i.e., without the supplementary superstructure spots) was solved in the space group $I4/m$ (a = 13.7588(7) Å, c = 5.6879(3) Å, R_F(obs) = 3.79%, wR_F(obs) = 4.49%, R_F(all) = 7.37%, wR_F(all) = 4.79%, with $I_{obs} > 3\sigma(I)$), leading to the formula $[Bi_{10}(Bi_{\sim0.5}Cd_{\sim0.5})_8{}^{dis}O_{16}](Bi_{0.6}Cd_{0.8})_2{}^{ord}(PO_4)_8$.

The crystal structure can be described by infinite square based columns (2 × 2 OBi_4 tetrahedra width) surrounded by eight isolated PO_4's and two tunnels formed by four PO_4 groups. In its formula, $(Bi_{\sim0.5}Cd_{\sim0.5})^{dis}$ stands for mixed sites at the corners of columns, whereas $(Bi_{0.6}Cd_{0.8})^{ord}$ is related to the occupancy of tunnels between phosphates as shown in Figure 4a. The refinement of mixed sites in tunnels is very

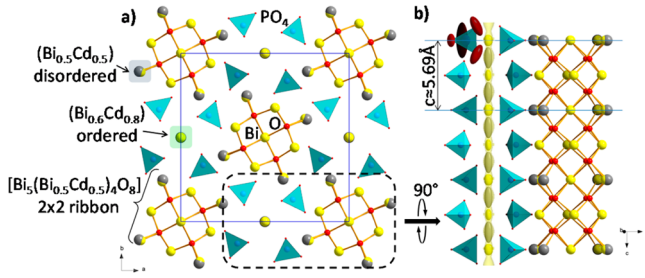

Figure 4. (a) Projection along the c axis of the average crystal structure of $[Bi_{10}(Bi_{\sim0.5}Cd_{\sim0.5})_8{}^{dis}O_{16}](Bi_{0.6}Cd_{0.8})_2{}^{ord}(PO_4)_8$ and (b) the square based columns and PO_4 tunnels along the c axis on the left (the yellow continuum along the tunnel is the electron density obtained after Fourier difference of the electron map without cation (30 $e^-/Å^3$).

approximate, two partially occupied sites (one Bi site and one Cd site) being distinct but assorted with very high anisotropic displacement parameters along the c axis (see Figure 4b). In this average structure, the observation of a continuum of electron density in the tunnel is shown in yellow (30 $e^-/Å^3$ isosurface) in Figure 4b, while the located Bi and Cd sites are also drawn.

Modulated Structure Approach. Further electron diffraction studies and XRD precession calculations enhance satellite reflections due to an incommensurate structural modulation (Figure 5). The tetragonal lattice parameters and the modulation vector were refined to $a = b$ = 13.768(4) Å, c = 5.691(2) Å, q = 0.000(1)a^*, 0.0003(9)b^*, and 0.3984(4)c^* from 5046 main reflections and 935 first and second order satellites using NADA.[27]

Note that for a second batch of single crystals, the modulation vector was refined to q = 0.000(4)a^*, 0.0005(4) b^*, and 0.4086(2)c^*, which validate the incommensurability ($q \neq 2/5$) and possible deviation from one specimen to another, possibly due to minor cationic distribution changes between the different mixed Bi/Cd sites. All reflections were integrated and indexed using the 4D formalism ($hklm$ spot corresponds to the point $hkl + mq$ of the reciprocal space). The observed satellite spots are limited to small indices (only few m_{max} = 2 reflexions

dx.doi.org/10.1021/ic402930d | Inorg. Chem. 2014, 53, 861−871

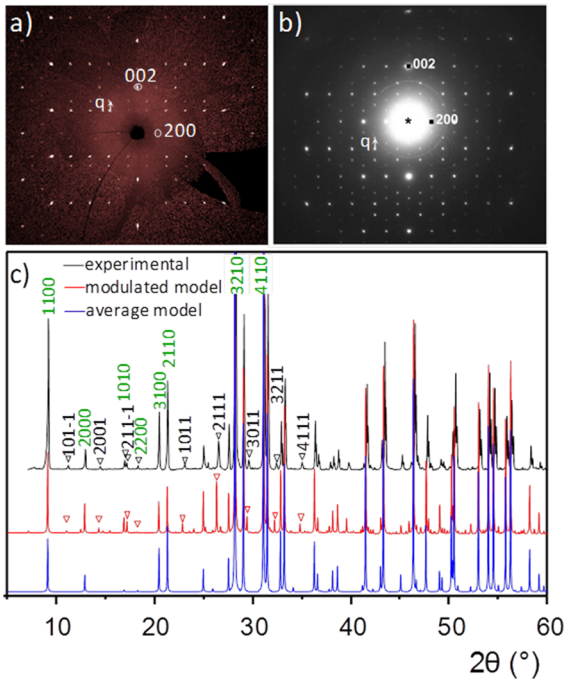

Figure 5. $[Bi_{10}(Bi_{\sim 0.5}Cd_{\sim 0.5})_8{}^{dis}O_{16}](Bi_{0.6}Cd_{0.8})_2{}^{ord}(PO_4)_8$: (a) Calculated precession of (*h*0*l*) layer (XRD on single crystal) and (b) ED image of (*h*0*l*) layer with enhancement of substructure spots ($q \approx 0.4$ c*). (c) The comparison between the calculated XRD patterns (average and modulated models) and the experimental one. Green indices are the fundamental and black ones are the modulation peaks.

are observed), which suggest, additionally to the common Bessel effect, a partial ordering with smooth atomic displacement along the fourth dimension. Taking into account the average space group ($I4/m$), the study of the *hklm* reflections shows the conditions *hklm*: $h + k + l = 2n$, 00*lm*: $m = 2n$ leading to only one possible superspace group $I4/m$(00-p)s0. This group is characterized by the translations (0000; 1/2 1/2 1/2 0) and equivalent coordinates: $x, y, z, x4$; $-x, -y, z, x4$; $-y, x, z, x4 + 1/2$; $y, -x, z, x4 + 1/2$; $-x, -y, -z, -x4$; $x, y, -z, -x4$; $y, -x, -z, x4 - 1/2$; $-y, x, -z, x4 - 1/2$, with $x4$ the coordinate along the fourth dimension. The study was performed in this space group using displacement and occupancy modulation waves. We note that lowering the symmetry or working in the 5-fold super cell in the approximation of a commensurate model did not change the results.

The continuum of density along the channel axis is broken in the 4D space where for each $x4$ value, Fourier peaks correspond to a particular value of z, which indicates a segregation of electronic densities in the fourth dimensional space (see Figure 6a and b). Several models have been tested, but only one converged. The study of the Fourier difference pertinent section in the ($x4$, z) map clearly evidences segments corresponding to Bi or Cd contributions along $x4$. To transfer this information into an atomic distribution, we used sawtooth functions which allow one to link a formal occupancy (present or absent) to a small atomic displacement Δz varying with $x4$. These occupancies appear in gray and yellow in Figure 6, which shows the Fourier difference in the pertinent section of the ($x4$, z) plane. At this level, the result of the refinement led to a total ordering of tunnels as shown in Figure 6c, showing a Bi/Cd ordering along c with the sequence $-$(Bi−Cd−Bi−Cd−Cd−Bi−Cd)$_n$− with distances between cations around 4 Å.

Using an identical process, we tried to distinguish segregation along the fourth dimension of mixed Bi3/Cd3 sites at the corners of columns. Figure 6e shows the electronic density calculated on Fourier difference maps along $x4$ at the concerned position. The more or less condensed density enhances variation of the local electronic density on this particular site. Here, we did not succeed in using the crenel of sawtooth functions that would point out a formal occupancy of Bi and Cd cations. Only smooth sinusoidal functions (related to a partial occupancy of Bi/Cd sites) were used to improve the refinement. Furthermore, without any additional constraint, the sinusoidal envelope of each individual Bi and Cd enhances a total occupancy of the crystallographic site with a ratio Bi/Cd ∼ 0.52:0.48. This is in good agreement with the 3D model of stoichiometry ($Bi_{\sim 0.5}Cd_{\sim 0.5}$) on this site. It indicates a partial disorder Bi/Cd of this site along z. All other atoms have been associated to first order modulated displacement functions, while for Bi1 and Bi2, modulated atomic displacement parameters have been considered, see Tables S4 and S5 for the details. The created PO_4 are nearly regular but remain associated with strong thermal parameters of oxygen corners. P−O distances have been constrained to 1.50(1) Å with ADP(O) restrained to 1.2xADP (P). At the end of the refinement, we obtain R_{fund} = 3.89%, $R_{sat\_order\ 1}$ = 10.97%, and $R_{sat\_order\ 2}$ = 13.37%. The final structural model clearly shows partial disorder on O(Bi,M)$_4$ tetrahedra of columns (probability of presence of Bi/Cd following sinusoidal distributions) and a Bi/Cd well established ordering in tunnels. The refined distances (average, minimum, and maximum) are listed in Table 3.

At least in this compound, between two mixed subunits, namely the cationic channels and the edges of oxocentered sites, the latter seems more adapted for disorder. Comparatively to results for the M = K case presented in the previous section, the M = Cd nature is of probable importance. Bi^{3+} and Cd^{2+} have similar ionic radii (0.95 Å), and due to the participation of a stereoactive lone pair in the coordination of the former and 4d orbitals for the latter, both require a particular bonding scheme by oxygen. The analysis of the coordination of the cations of the channels show differences between Bi and Cd. For Bi, the coordination number is either 6 or 8 with Bi−O distances between 2.4 and 2.8 Å, see Figure 6d. We note for the 8-fold coordination that the lone pair stereoactivity is not apparent in a rough approximation. Cd atoms are in a more or less distorted square planar coordination (Cd−O: 4 × 2.3 Å on average). The difference between these coordination polyhedra may be part of the driving force for the full cationic ordering in the channels. Differently at the edges of columns, the disordered Bi/Cd atoms have a greater coordination number (from 6 to 8). In such an environment, both Cd and Bi cohabit without ordering.

A perfect ordering of channel hosts in PO_4 tunnels was already previously observed, but in a compound with infinite planes instead of ribbons, namely $Bi_4ZnP_2O_{12}$, where the doubling of the b parameters of ∼2 × 5.4 Å is due to the ordered occupancy of channels by two independent Zn atoms in coordination IV and V, respectively.[9] However, in this latter compound, all sites of the polycationic infinite layers are solely occupied by Bi^{3+} atoms, and channels are occupied solely by Zn^{2+} ions. In addition, in our prior TEM investigation of compounds with various-sized ribbons with mixed Bi/M sites at their edges, it is common to evidence some superstructures commensurate or incommensurate. However, this information

dx.doi.org/10.1021/ic402930d | Inorg. Chem. 2014, 53, 861−871

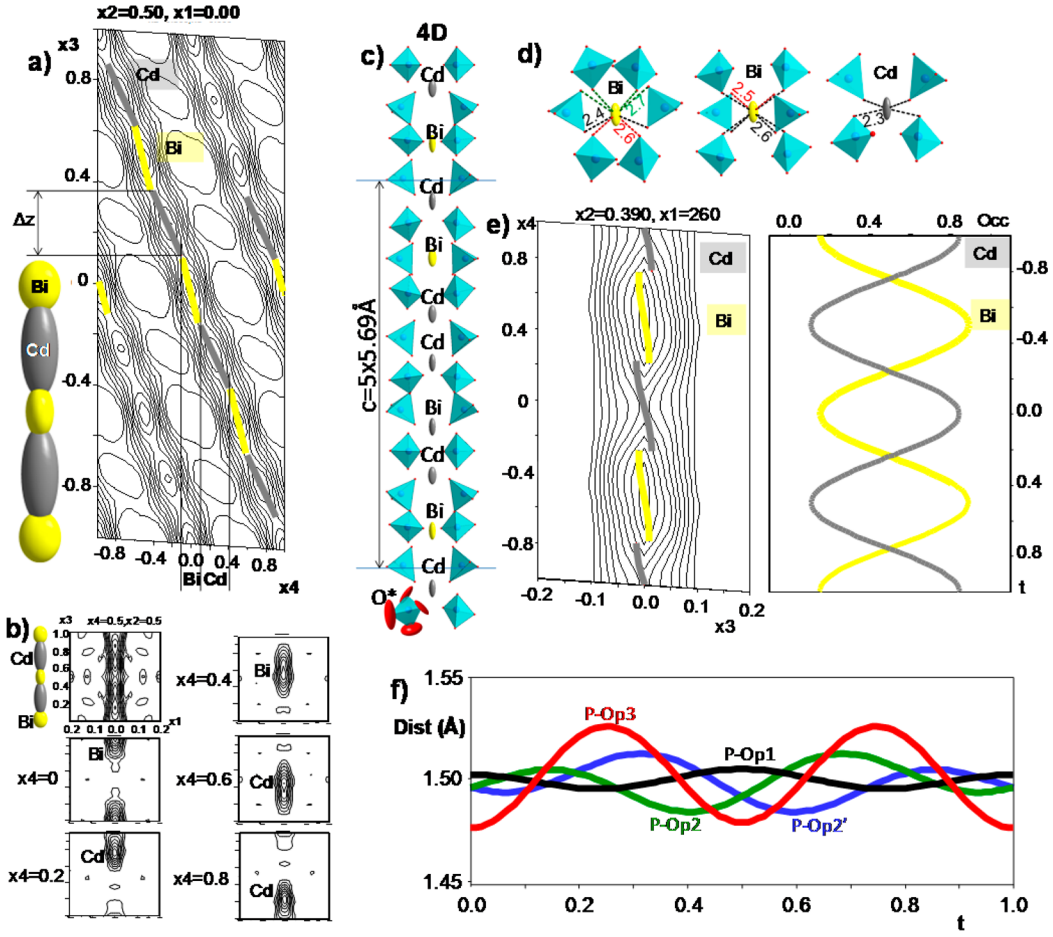

Figure 6. (a) Fourier difference along ($x4$, z) in the tunnel (contribution from $x4$ = 0 to 1 are summed). (b) Separation of two sites Bi/Cd at different sections along $x4$. (c) Bi/Cd repartition in the modulated structure of $[Bi_{10}(Bi_{\sim 0.5}Cd_{\sim 0.5})_8{}^{dis}O_{16}](Bi_{0.6}Cd_{0.8})_2{}^{ord}(PO_4)_8$. The asterisk (∗) corresponds to the following: the anisotropic displacement shown at the bottom for PO_4 concerns a refinement in the absence of restraint on the oxygen ADP and validates a disordered sketch. (d) coordination of Bi and Cd in the channel. (e) An electronic density and occupancy of Bi/Cd sites of the columns. (f) P−O bond distances along the fourth dimension real-space projected coordinate t.

Table 3. Interatomic Distances (Å) of the Atoms on the Edges of the Ribbons and in the Cationic Channels of $[Bi_{10}(Bi_{\sim 0.5}Cd_{\sim 0.5})_8{}^{dis}O_{16}]$ $(Bi_{0.6}Cd_{0.8})_2{}^{ord}(PO_4)_8$

atom 1	atom 2	$d_{average}$	d_{min}	d_{max}
Bi1	4xO1	2.243(12)	2.183(12)	2.343(12)
Bi2	8xO1	2.497(12)	2.412(12)	2.585(12)
Bi3	2xO1	2.296(13)	2.206(13)	2.385(13)
	Op1	2.25(2)	2.19(3)	2.31(3)
	2xOp2	2.43(2)	2.26(2)	2.65(2)
	Op3	2.56(2)	2.28(3)	2.69(2)
Cd3	2xO1	2.201(16)	2.073(17)	2.327(18)
	Op1	2.41(3)	2.35(3)	2.46(3)
	2xOp2	2.58(2)	2.39(3)	2.81(2)
	Op3	2.40(3)	2.14(4)	2.52(2)
Bia	8xOp2	2.56(2)	2.38(3)	2.77(4)
Cdb	4xOp2	2.32(2)	2.25(2)	2.35(2)
P	Op1	1.48(2)	1.43(3)	1.55(3)
	2xOp2	1.50(2)	1.36(2)	1.63(2)
	Op3	1.60(3)	1.52(3)	1.68(2)

is often lost on the single crystal scale. It follows that their origin remains mysterious, even if one has to keep in mind the case of $Bi_{\sim 6.2}Cu_{\sim 6.2}O_8(PO_4)_5$, where HREM images of modulated zones clearly indicate that ordering phenomena occur in the Cu^{2+} tunnels between double (n = 2O(Bi,M)$_4$-tetrahedra-long) and triple (n = 3O(Bi,M)$_4$-tetrahedra-long) ribbons.[28] These features comfort a better suitability for ordering in tunnels rather (at least in microdomains) than mixed positions belonging to oxocentered subunits. However, in the title $[Bi_{10}(Bi_{\sim 0.5}Cd_{\sim 0.5})_8{}^{dis}O_{16}](Bi_{0.6}Cd_{0.8})_2{}^{ord}(PO_4)_8$ compound, the partial ordering was also observed in a polycrystalline sample, even if the small change of modulation vector pictures local compositional variations, as discussed above, Figure 5.

3. Full Cationic Ordering in $[Bi_{18}Zn_{10}O_{21}]^{ord}Zn_5^{ord}(PO_4)_{14}$. This composition corresponds, in fact, to analogous compounds with M = Co and Mn originally considered as strongly disordered compounds, in the absence of supercell spots, leading to the formula $Bi_{\sim 1.2}M_{\sim 1.2}O_{1.5}(PO_4)$.[14] It consists of n = 3-tetrahedra wide ribbons with mixed Bi/M sites at their edges. A strong disorder over M^{2+} hosts was observed in the tunnels while the oxygen coordination of P atoms was also very disordered, due to the superposition of several PO_4 configurations. For M = Zn, XRD powder pattern refinement leads to a similar subcell (a = 14.809(2) Å, b = 11.214(1) Å, c = 5.440(1) Å, S.G. *Ibam*) and identical $Bi_{\sim 1.2}Zn_{\sim 1.2}O_{1.5}(PO_4)$ formula assumption. In this previous study, no evidence of supercell ordering was detected on the used single crystals, while ED patterns on $Bi_{\sim 1.2}M_{\sim 1.2}O_{1.5}(PO_4)$ (M = Zn, Mn, and

dx.doi.org/10.1021/ic402930d | *Inorg. Chem.* 2014, 53, 861−871

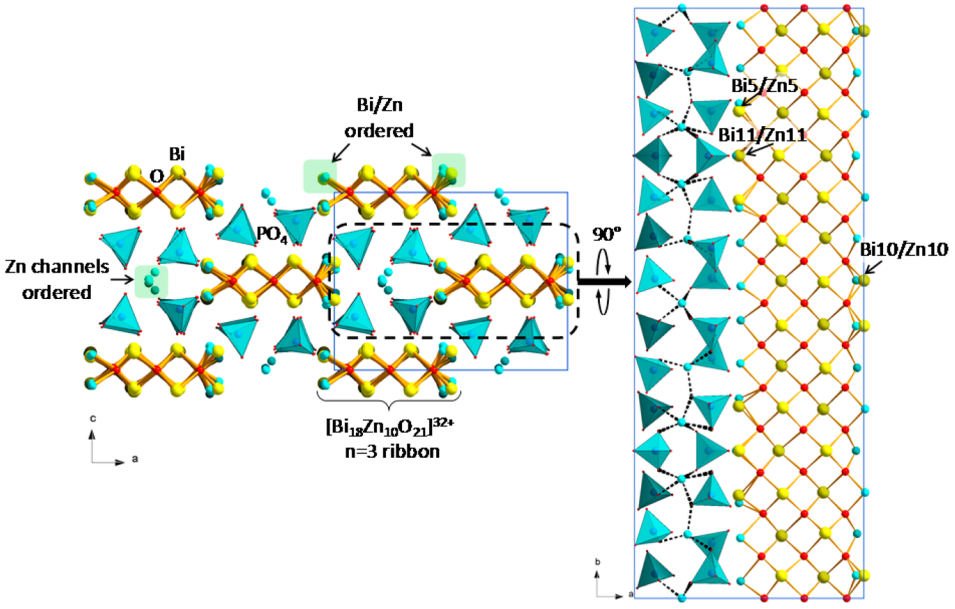

Figure 7. The crystal structure of $[Bi_{18}Zn_{10}O_{21}]^{ord}Zn_5^{ord}(PO_4)_{14}$ (projection along *b* axis) on the left and the ribbon and PO_4 tunnel (projection along *c* axis) on the right.

Co) show clues for inhomogeneity in the sample with sometimes the presence or not of additional spots (in commensurate or incommensurate positions) or diffuse lines. In the frame of this study, we have prepared single crystals of the Zn compound as detailed in the Experimental Section.

The single crystal structure was solved in the *I*2*mb* space group (a = 14.8003(1) Å, b = 38.0848(2) Å, c = 11.2473(5) Å, R_1 = 3.7%, wR_2 = 4.0%). In fact, as we will see later, this compound shows a nearly perfect ordering of the cations and PO_4 groups in the structure. Indeed, in the tunnels, three fully occupied independent Zn cations are ordered along the 7*xb* periodicity as shown in Figure 7, with no residual electronic density on Fourier-difference maps. The coordination of Zn^{2+} is IV or V, while the Zn−Zn distances are between 3.62 Å and 4.18 Å. The oxygen of the bordering PO_4 groups has normal thermal parameters which validate the perfect ordering inside the channels. Concerning the ribbon edges, the situation is less clear but remains very close to a perfect ordering.

In fact, as shown in Figure 7, most of the positions are fully occupied by Zn^{2+}, while only three mixed sites (out of eight), Bi11(32%)/Zn11(68%), Bi5(90%)/Zn5(10%), and Bi10(94%)/Zn10(6%), contain a significant amount of Bi^{3+}. On the basis of the residual Fourier peaks, these sites are occupied by Bi and Zn at distinct adjacent sites. The refinement of their occupancies lead, without any constraint, to an electroneutral solid of formula $Bi_{17.95}Zn_{14.69}O_{21}(PO_4)_{14}$. Note also that BVS calculations show that both Zn^{2+} and Bi^{3+} are suitably coordinated by the surrounding PO_4 groups, see Table 4.

Only in the mixed Bi11/Zn11 position, despite the splitting of the two types of cations, does Bi^{3+} seem overbonded (BVS = 4.27), which involves the mean position being dominated by its major Zn character. It leads to a complex sequence of Bi/Zn and Zn along the ribbon axis as shown in Figure 7. The perfect and almost perfect cationic ordering in the tunnels and inside oxocentered sites respectively validate what was deduced in the previously presented compound. In this almost fully ordered compound, it is probable that the Zn/Bi ordering is driven by the very different chemical nature of both elements. For Zn^{2+}, the coordination sphere is mediated by its d orbitals while Bi 6p/6s states create the asymmetric BiO_n coordination. The selected distances are given in Table 5.

Table 4. Calculated BVS of Selected Atoms in $[Bi_{18}Zn_{10}O_{21}]^{ord}Zn_5^{ord}(PO_4)_{14}$

atom	BVS	atom	BVS
Bi1	2.91(3)	Zn10	1.71(14)
Bi2	2.94(4)	Bi11	4.27(13)
Bi3	2.99(3)	Zn11	1.78(8)
Bi4	2.88(4)	Zn1	2.02(3)
Bi5	3.13(4)	Zn2	1.92(4)
Zn5	1.68(9)	Zn3	2.04(4)
Bi6	2.98(3)	Zn4	1.97(3)
Bi7	2.85(4)	Zn9	1.94(4)
Bi8	3.05(3)	Zn6	1.98(4)
Bi9	2.91(4)	Zn7	2.04(7)
Bi10	3.02(3)	Zn8	2.09(4)

The precession image (XRD data) of the single crystal (Figure 8a) evidences a commensurate 7-fold supercell along the channel axis (0*kl* layer). At least, the ED patterns of the [001] zone axis on crystals of the powder sample shows evidence of supercell spots (Figure 8b), but their intensities are much weaker than found in the single-crystal precession frame. In fact, this contrast is different from one crystallite to the other and suggests that these ordered domains occur only on a nanometric scale and that the extension of the cation ordering on a greater scale is broken, probably by antiphase boundaries. Indeed, the XRD pattern shows that supercell lines are lost on the scale of micronic grains (see Figure 8c). Therefore, the studied fully ordered single crystal should be considered as a rare opportunity.

We have also performed ^{31}P NMR experiments on the prepared polycrystalline sample (see Figure 3b). An accurate best-fit simulation into the different types of phosphorus environments is outside the scope of the present work, due to strong overlapping of resonances. However, the overall line

dx.doi.org/10.1021/ic402930d | *Inorg. Chem.* 2014, 53, 861−871

Table 5. Selected Interatomic Distances (Å) of $[Bi_{18}Zn_{10}O_{21}]^{ord}Zn_5^{ord}(PO_4)_{14}$

atom 1	atom 2	d	atom 1	atom 2	d	atom 1	atom 2	d
Bi5	1xO9	2.104(16)	Bi11	1xOp3c	1.941(42)	Zn4	1xOp6d	2.022(16)
	1xO10	2.245(16)		2xO10	2.198(23)		1xO12	2.055(16)
	1xOp5b	2.304(16)		1xOp8a	2.199(32)		1xOp7b	2.061(16)
	1xOp7b	2.367(16)		2xOp5a	2.257(23)		1xOp2a	2.112(14)
	1xOp4b	2.470(19)	Zn11	1xOp3c	2.067(49)		1xOp5b	2.190(16)
Zn5	1xO9	1.903(36)		1xOp8a	2.085(41)		1xO9	2.344(16)
	1xOp7b	1.907(41)		2xOp5a	2.132(28)	Zn6	1xOp7a	1.900(17)
	1xOp5b	2.264(37)		2xO10	2.288(29)		1xOp6c	1.935(16)
	1xOp4b	2.283(38)	Zn1	1xOp7c	1.967(16)		1xOp5c	2.000(16)
	1xO10	2.608(39)		1xOp1b	2.063(16)		1xOp2a	2.042(14)
Bi10	1xO5	2.115(15)		1xO7	2.121(15)	Zn7	1xOp8b	1.895(33)
	1xO6	2.181(90)		1xOp2b	2.143(15)		1xOp3a	1.997(23)
	1xOp2d	2.409(15)		1xOp2b	2.156(16)		1xOp4d	2.016(18)
	1xOp1c	2.540(14)		1xO12	2.254(16)		1xOp5c	2.045(16)
	1xOp6d	2.627(16)	Zn2	2xOp4c	2.018(17)		1xOp5a	2.399(17)
	1xOp1b	2.656(16)		2xO11	2.078(13)	Zn8	2xOp2c	1.868(16)
	1xOp6c	2.709(16)		1xOp8c	2.116(24)		2xOp1c	2.039(15)
Zn10	1xO5	1.900(51)	Zn3	1xOp1d	1.904(16)	Zn9	1xOp6b	1.949(16)
	1xOp2d	1.954(58)		1xO8	1.985(13)		1xO11	2.027(13)
	1xO6	2.003(50)		1xOp7d	2.105(16)		1xO8	2.066(13)
	1xOp6d	2.653(51)		1xOp4b	2.119(19)		1xOp4d	2.116(18)
	1xOp1b	2.719(52)		1xO5	2.121(15)		1xOp3a	2.153(23)

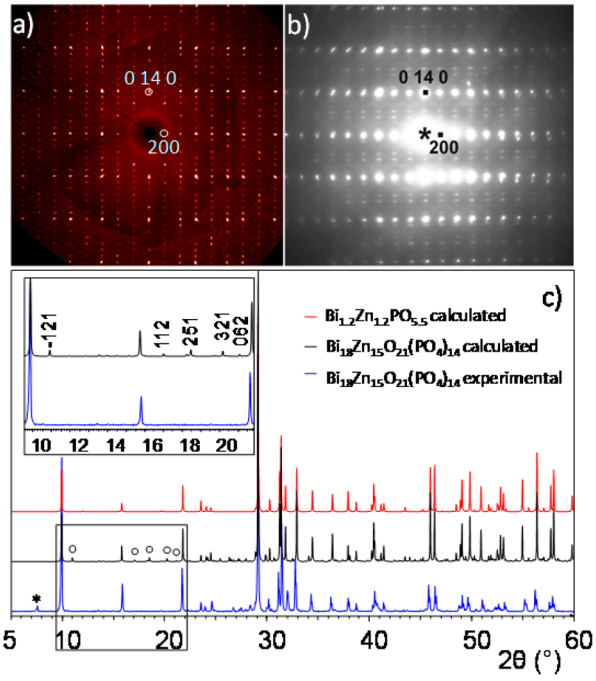

Figure 8. (a) Calculated precession frame from single crystal XRD data of $[Bi_{18}Zn_{10}O_{21}]^{ord}Zn_5^{ord}(PO_4)_{14}$. (b) ED patterns of the 0*kl* layer of the corresponding powder and (c) XRD patterns calculated from the disordered structure of $Bi_{1.2}Zn_{1.2}O_{1.5}PO_4$ (red), from the ordered single crystal of $[Bi_{18}Zn_{10}O_{21}]^{ord}Zn_5^{ord}(PO_4)_{14}$ (black) and experimental (blue). Inset: selected 2θ range showing some superstructure peaks—a sign of cation ordering. (∗) Indicates an unidentified peak.

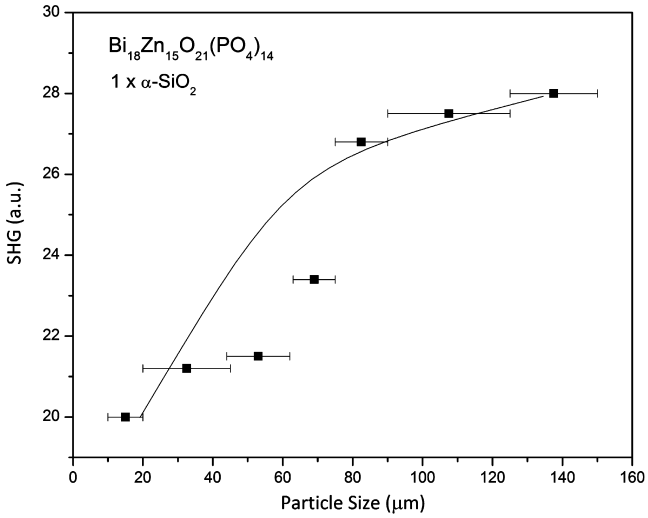

Figure 9. SHG response vs particle size of $[Bi_{18}Zn_{10}O_{21}]^{ord}Zn_5^{ord}(PO_4)_{14}$. The line is drawn to guide the eye and is not a fit to the data.

shape follows a Lorentzian pattern, confirming the high level of cationic ordering.

Powder SHG measurements on $[Bi_{18}Zn_{10}O_{21}]^{ord}Zn_5^{ord}(PO_4)_{14}$ were performed using 1064 nm radiation. The SHG results are shown in Figure 9. The material has an SHG efficiency approximately equal to α-SiO_2, confirming that the bulk material conserves its noncentrosymmetric character refined from single crystal XRD data, despite the loss of full-ordering deduced from powder XRD data. In addition, particle size versus SHG efficiency revealed that the material is type 1 phase-matchable, which means that the fundamental and second-harmonic wavelengths constructively add as the light propagates through the material. The small residual crystallographic disorder between the Bi^{3+} and Zn^{2+} cations is a likely reason for the relative weak SHG response and may be related to the bad matching between the expected and observed particle-size dependent response.

CONCLUDING REMARKS, STRUCTURAL FLEXIBILITY AND GRADUAL ORDERING

As already discussed in previous papers, these compounds can be considered as derivatives of the fluorite-like δ-Bi_2O_3 crystal

dx.doi.org/10.1021/ic402930d | Inorg. Chem. 2014, 53, 861−871

structure in terms of their cationic arrangement. M and P atoms substitute the Bi positions while the resulting network is strongly distorted, for instance due to the incorporation of extra-oxygen atoms with PO_4 groups. Using this description, the cationic channels can be considered as interstitial sites between PO_4 groups. This fluorite heritage is of primal importance, since the notion of substitution of cations of groups for Bi^{3+} guarantees the conservation of the cationic content, on the basis of the possible prediction, formulation, and preparation of hypothetical members intensively studied by our group.[8−11] The 2D projection of the lattice perpendicularly to the ∼5.5 Å axis (or supercell related lattice parameter) helps to view the distortion due to the incorporation of PO_4 and allows one to distinguish the topology of oxocentered tetrahedra preserved from the parent fluorite. In such a sketch, two next cations (Bi^{3+}, Bi^{3+}/M^{n+}, P^{5+}) along horizontal and vertical grid-lines occupy x (in plane) and $x + 1/2$ (out of plane) in regard to the ∼5.5 Å parameter. Such 2D-cationic projections have already been drawn and discussed for noncentrosymmetric compounds with n = 5, 8, and 11 tetrahedra-wide ribbons[8] and for compounds with infinite layers.[10] In these compounds, the oxocentered units (ribbons or plane run parallel, and PO_4 fulfills the available lattice sites. The same construction for $[Bi_{18}Zn_{10}O_{21}]^{ord}Zn_5^{ord}(PO_4)_{14}$ is shown in Figure 10a where oxocentered units are highlighted in yellow. Compared to the ideal square grid for δ-Bi_2O_3, it is clear that the PO_4-rich area between the ribbons is strongly distorted in agreement with the important concentration of voluminous phosphate groups. We recall that the tunnel hosts are considered interstitial and are not assigned to a particular x coordinate.

A similar construction for $[Bi_2(Bi_{1.56}K_{0.44})^{dis}O_3]K_{0.88}{}^{dis}(PO_4)_2$ is shown in the Figure 10b. Here, similar n = 3 ribbons are arranged according to a 4-fold axis, but clearly the distortion of the ideal-square lattice is weakly distorted by PO_4 compared to the previous case. In fact, close inspection of the z coordinates indicate that the building of horizontal and vertical lines of the grid involves the creation of cationic vacancies around the tunnels. It is inherent to the perpendicular disposition of the oxocentered units, and most probably these "virtual" vacancies allow the relaxation of the structure and are responsible for the regular 2D lattice.

For $[Bi_{10}(Bi_{\sim 0.5}Cd_{\sim 0.5})_8{}^{dis}O_{16}](Bi_{0.6}Cd_{0.8})_2{}^{ord}(PO_4)_8$, as shown in Figure 10c, once more, vacancies relax the structure into a regular lattice. However, the concentration of oxocentered tetrahedra into square columns seems to favor a more distorted PO_4 surrounding, compared to $[Bi_2(Bi_{1.56}K_{0.44})^{dis}O_3]K_{0.88}{}^{dis}(PO_4)_2$ despite a smaller ratio of $O(Bi,M)_4/PO_4$, i.e., 2 for the former against 3/2 for the latter. According to this descriptive type, we observe a periodic lattice of cations that form the nodes of the cationic grid, with an external cationic disorder in terms of occupancy (external Bi/M sites of oxocentered units).

According to our experience, the shape of the resulting oxocentered units can be anticipated for very accurate compositions in the case of parallel 1D ribbons.[8,9] In general cases, it is ruled out by the $O(Bi,M)_4/PO_4$ ratio and by the M cocation charge for electroneutrality. However, "atypic" oxocenterd units (e.g., square columns) or nonparallel arrangements (tetragonal symmetry) are difficult to predict. For instance, in $[Bi_2(Bi_{1.56}K_{0.44})^{dis}O_3]K_{0.88}{}^{dis}(PO_4)_2$ we find $O(Bi,M)_4/PO_4$ = 3/2 leading to 3-$O(Bi,M)_4$ sized ribbons perpendicular to each other in the presence of K^+. In

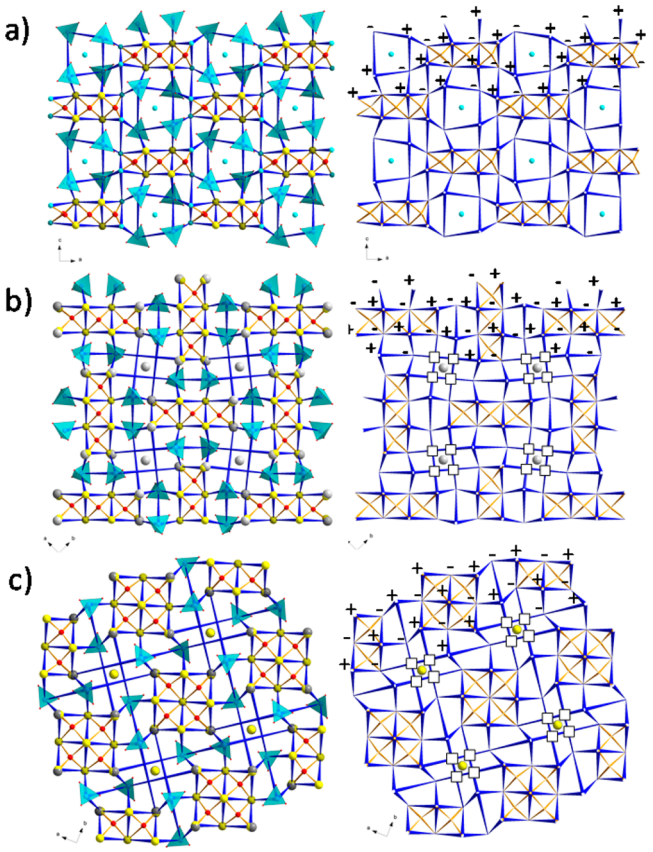

Figure 10. Cationic grid representation of the structures of (a) $[Bi_{18}Zn_{10}O_{21}]^{ord}Zn_5^{ord}(PO_4)_{14}$, (b) $[Bi_2(Bi_{1.56}K_{0.44})^{dis}O_3]$-$K_{0.88}{}^{dis}(PO_4)_2$, and (c) $[Bi_{10}(Bi_{\sim 0.5}Cd_{\sim 0.5})_8{}^{dis}O_{16}]$-$(Bi_{0.6}Cd_{0.8})_2{}^{ord}(PO_4)_8$. Minus (−) and plus (+) signs indicate x and $x + 1/2$ "out-of-plane," respectively, with regard to a ∼5.5 Å parameter. The tunnel hosts are shown on both representations and are interstitial cations. In b and c, small open squares show the virtual cationic vacancies.

$[Bi_{18}Zn_{10}O_{21}]^{ord}Zn_5^{ord}(PO_4)_{14}$, we also have $O(Bi,M)_4/PO_4$ = 3/2 but with similar oxocentered units arranged parallel to each other, in the presence of Zn^{2+}. This point shows an important limit about structural prediction in these systems.

To understand the "easy" random distribution on edges of oxocentered units, one should observe the geometries of the oxocentered $O(Bi,Zn)_4$ tetrahedra in $[Bi_{18}Zn_{10}O_{21}]^{ord}Zn_5^{ord}$-$(PO_4)_{14}$. They display various distortions due to the differences between Zn−O (1.90 Å) and Bi−O (2.24 Å) distances which create local constraints and relaxations. At least it seems that the flexibility of oxocentered poly units is sufficiently important to self-adapt Bi/M mixed sites in a fully disordered manner ($[Bi_2(Bi_{1.56}K_{0.44})^{dis}O_3]K_{0.88}{}^{dis}(PO_4)_2$ and $[Bi_{10}(Bi_{\sim 0.5}Cd_{\sim 0.5})_8{}^{dis}O_{16}](Bi_{0.6}Cd_{0.8})_2{}^{ord}(PO_4)_8$) or in almost ordered manner as in the case of $[Bi_{18}Zn_{10}O_{21}]^{ord}Zn_5^{ord}$-$(PO_4)_{14}$.

Only PO_4 corners and their in-channel neighbors are disordered over several strongly split positions (K^+ case) or order with respect to long periodicities perpendicularly to the projection axis (Zn^{2+} and Bi^{3+}/Cd^{2+} cases). Our results seem to confirm the general idea that in this family of compounds a simple periodic skeleton of $O(Bi,M)_4$ units is holding the crystal structure while the surrounding space is filled by more or less disordered counterions including interstitial ions. Slight compositional changes seem to modify the interstitial

dx.doi.org/10.1021/ic402930d | Inorg. Chem. 2014, 53, 861−871

sublattice, while the main oxocentered sublattice is not sensitively modified.

■ ASSOCIATED CONTENT

Supporting Information

^{31}P double quantum MAS spectrum, experimental XRD pattern, fractional atomic coordinates and isotropic or equivalent isotropic displacement parameters, atomic displacement parameters, fractional atomic coordinates and isotropic or equivalent isotropic displacement parameters, BVS values of selected atoms, and crystallographic information files. This material is available free of charge via the Internet at http://pubs.acs.org.

■ AUTHOR INFORMATION

Corresponding Author

*E-mail: Olivier.mentre@ensc-lille.fr.

Notes

The authors declare no competing financial interest.

■ ACKNOWLEDGMENTS

The Fonds Européen de Développement Régional (FEDER), CNRS, Région Nord Pas-de-Calais, and Ministére de l'Education Nationale de l'Enseignement Supérieur et de la Recherche are acknowledged for funding the X-ray diffractometers. Laurence Burylo and Nora Djellal are thanked for their precious technical help. This work was carried out under the framework of the Multi-InMaDe project supported by the ANR (Grant ANR 2011-JS-08 003 01). TTT and PSH thank the Welch Foundation (Grant E-1457) for support.

■ REFERENCES

(1) Krivovichev, S. V.; Mentré, O.; Siidra, O. I.; Colmont, M.; Filatov, S. K. *Chem. Rev.* **2013**, *113* (8), 6459−6535.

(2) Krivovichev, S. V.; Filatov, S. K. *Crystal Chemistry of Minerals and Inorganic Compounds with Complexes of Anion-Centered Tetrahedra*; St. Petersburg University Press: St. Petersburg, Russia, 2001.

(3) Muktha, B.; Guru Row, T. N. *Struct. Chem.* **2006**, *18*, 195−202.

(4) Enjalbert, R.; Hasselmann, G.; Galy, J. *Acta Crystallogr., Sect. C* **1997**, *53*, 269−272.

(5) Landa-Cánovas, Á. R.; Vila, E.; Hernández-Velasco, J.; Galy, J.; Castro, A. *Acta Crystallogr., Sect. B* **2009**, *65*, 458−466.

(6) Hyman, A.; Perloff, A. *Acta Crystallogr., Sect. B* **1972**, *28*, 2007−2011.

(7) Colmont, M.; Huvé, M.; Ketatni, E. M.; Abraham, F.; Mentré, O. *J. Solid State Chem.* **2003**, *176*, 221−233.

(8) Endara, D.; Colmont, M.; Huvé, M.; Capet, F.; Lejay, J.; Aschehoug, P.; Mentré, O. *Inorg. Chem.* **2012**, *51*, 9557−9562.

(9) Endara, D.; Colmont, M.; Huvé, M.; Tricot, G.; Carpentier, L.; Mentré, O. *Inorg. Chem.* **2012**, *51*, 4438−4447.

(10) Colmont, M.; Endara, D.; Aliev, A.; Terryn, C.; Huvé, M.; Mentré, O. *J. Solid State Chem.* **2013**, *203*, 266−272.

(11) Huvé, M.; Colmont, M.; Lejay, J.; Aschehoug, P.; Mentré, O. *Chem. Mater.* **2009**, *21*, 4019−4029.

(12) Cornei, N.; Tancret, N.; Abraham, F.; Mentré, O. *Inorg. Chem.* **2006**, *45*, 4886−4888.

(13) Kozin, M. S.; Colmont, M.; Endara, D.; Aliev, A.; Huvé, M.; Siidra, O. I.; Krivovichev, S. V.; Mentré, O. *J. Solid State Chem.* **2013**, *199*, 123−128.

(14) Abraham, F.; Cousin, O.; Mentre, O.; Ketatni, E. M. *J. Solid State Chem.* **2002**, *167*, 168−181.

(15) Colmont, M.; Delevoye, L.; Mentré, O. *New J. Chem.* **2009**, *33*, 19−22.

(16) Colmont, M.; Huvé, M.; Abraham, F.; Mentré, O. *J. Solid State Chem.* **2004**, *177*, 4149−4162.

(17) Cousin, O.; Huve, M.; Roussel, P.; Perez, O.; Steinfink, H. *J. Solid State Chem.* **2002**, *165*, 324−333.

(18) *SAINT: Area-Detector Integration Software*; Siemens Industrial Automation, Inc.: Madison, WI, 1996.

(19) *SADABS: Area-Detector Absorption Correction*; Siemens Industrial Automation, Inc.: Madison, WI, 1995.

(20) Palatinus, L.; Chapuis, G. *J. Appl. Crystallogr.* **2007**, *40*, 786−790.

(21) Petricek, V.; Dusek, M.; Palatinus, L. *Jana2006. The crystallographic computing system*; Institute of Physics: Praha, Czech Republic, 2006.

(22) Rodriguez-Carvajal, J. *Comm. Powder Diffr. (IUCr) Newslett.* **2001**, *26*, 12−19.

(23) Ok, K. M.; Chi, E. O.; Halasyamani, P. S. *Chem. Soc. Rev.* **2006**, *35*, 710−717.

(24) Colmont, M.; Delevoye, L.; Ketatni, E. M.; Montagne, L.; Mentré, O. *J. Solid State Chem.* **2006**, *179*, 2111−2119.

(25) Sanderson, R. T. *Polar Covalence*; Academic Press: Waltham, MA, 1983.

(26) Mentre, O.; Roussel, P.; Petricek, V. Private Communication.

(27) Schönleber, A.; Meyer, M.; Chapuis, G. *J. Appl. Crystallogr.* **2001**, *34*, 777−779.

(28) Ketatni, E. M.; Huvé, M.; Abraham, F.; Mentré, O. *J. Solid State Chem.* **2003**, *172*, 327−338.